J Appl Electrochem (2009) 39:1229–1236
DOI 10.1007/s10800-009-9787-4

ORIGINAL PAPER

Effects of electrospun polyacrylonitrile-based carbon nanofibers as catalyst support in PEMFC

Jae-Hyun Park · Young-Wan Ju · Seok-Hwan Park · Hong-Ryun Jung · Kap-Seung Yang · Wan-Jin Lee

Received: 14 March 2008 / Accepted: 6 January 2009 / Published online: 20 January 2009

Abstract This paper reports novel results regarding the effects of electrospun carbon nanofibers (e-CNF) as a catalyst support by comparison with the commercial Vulcan XC-72R (denoted as XC-72R) as granular particles. The e-CNF was synthesized by stabilizing and carbonizing the electrospun PAN-based fibers. The e-CNF showed an average diameter of 250 nm with a rough surface and was partially aligned along the winding direction of the drum winder. The characteristic morphology was fundamentally dependant on the shape of the carbon materials. The average pore size of the e-CNF was 2.36 nm, while that of the XC-72R was 10.92 nm. The morphology of e-CNF was developed by shallow pores with rough surfaces due to the effects of electrospinning and carbonization, while that of the XC-72R was largely developed by mesopores rather than micropores due to the granular shape. Compared to XC-72R, the performance of the MEA prepared by e-CNF was excellent, owing to the morphology and the enhanced electrical conductivity. The Pt utilization of Pt/e-CNF was 69%, while that of Pt/XC-72R was 35%.

Keywords Electrospinning · Carbonization · Carbon nanofibers · Morphology · Pt utilization

J.-H. Park · Y.-W. Ju · S.-H. Park · H.-R. Jung · K.-S. Yang · W.-J. Lee (✉)
Faculty of Applied Chemical Engineering, Chonnam National University, 300 Yongbong-dong, Buk-gu, Gwangju 500-757, Korea
e-mail: wjlee@jnu.ac.kr

J.-H. Park · Y.-W. Ju · S.-H. Park · H.-R. Jung · K.-S. Yang · W.-J. Lee
Center for Functional Nano Fine Chemicals, Chonnam National University, 300 Yongbong-dong, Buk-gu, Gwangju 500-757, Korea

1 Introduction

Polymer electrolyte membrane fuel cells (PEMFC) have received extensive attention as promising power source candidates for various applications such as low emission vehicles, distributed home power generation, and back-up sources for small portable electronics due to their high efficiency, cleanliness, and quiet operation [1–3]. The performance of the catalyst support in the PEMFC is closely dependant on the morphology of the carbon materials in the support and the dispersion of the catalyst [4–8]. In general, commercial Vulcan XC-72R (referred to as XC-72R) is commonly used as a PEMFC catalyst support. However, this carbon material has a tendency to restrict PEMFC performance given its simultaneous lack of high surface area and very shallow pores, despite its well-developed rough surface. However, XC-72R bearing deep mesopores easily allows Pt particles to penetrate into the mesopores to deter the formation of a three-phase boundary by preventing the Nafion ionomer (4–200 nm diameter) from contacting the Pt particles deep within the mesoporous XC-72R [6, 9]. Accordingly, shallow porous carbon material can enhance performance by inducing close contact between the Pt particles supported on the carbon and Nafion ionomer.

Generally, the morphology of carbon nanofibers varies with thermal pyrolysis conditions such as carbonization and activation [10–12]. In the process of activation, carbon nanofibers are formed bearing a high surface area with deep micropores or mesopores, such as an inkbottle shape. However, even in the case of high surface area, it is not as sufficient as Pt-supported carbon materials in enhancing PEMFC performance given its lack of a three-phase boundary consisting of a gas, an ion conductor and a catalyst. As a result, deep micropores inhibit the use of the

abundant surface area within the catalyst support and the deep mesopores subsequently permit facile penetration by the Pt particles.

However, in the process of carbonization, carbon nanofibers are formed with a morphology consisting of very shallow pores with a rough surface and as such it would be a suitable method for improving PEMFC performance by enhancing the three-phase boundary, as shallow pores with rough surfaces increase Pt utilization. Accordingly, the key to PEMFC performance enhancement is largely governed by the morphology and properties of the carbon materials used as the catalyst support [4–8].

Herein, we propose a novel method for improving PEMFC performance through control of the morphology of carbon through electrospinning and carbonization. The aligned e-CNF, prepared through the process electrospinning and carbonization, provides the improvement in PEMFC performance as follows. First, the e-CNF has a shallow and unique microstructure because of its submicron diameter. Second, the e-CNF has both a high surface area and very shallow pores with a rough surface. The fibrous nature of the aligned e-CNF also offers a high surface area with good connections between the catalytic particles in the reaction layer, bringing about improvement in Pt utilization by offering a good three-phase boundary. Third, the aligned e-CNF leads to high electronic conductivity by minimizing energy loss because the electrons transfer easily along the aligned e-CNF. Little attention, however, has been focused on methods of enhancing the PEMFC performance by preparing carbonized, electrospun e-CNF.

An aim of this study is to prepare carbonized electrospun polyacrylonitrile (PAN)-based carbon nanofiber (e-CNF) to improve PEMFC performance and replace commercial Vulcan XC-72R. The improvement in PEMFC performance is obtained by applying electrospinning and carbonization to create good morphology. The aligned CNF prepared by electrospinning and carbonization provides good morphology and acceptable catalytic properties as support for PEMFC.

2 Experimental

2.1 Preparation of carbonized e-CNF

Polyacrylonitrile-based fibers (PAN, Aldrich Chemical Co., St. Louis, MO, USA) were prepared by electrospinning. A 10 wt% PAN polymer solution in *N*,*N*-dimethylformamide (DMF, Aldrich Chemical Co.) was gently stirred for 24 h at 60 °C in order to obtain a homogeneous solution. Electrospinning of the solution was carried out by a previously described procedure [10–14]. The electrospun fibers were stabilized by heating to 280 °C at a rate of 1 °C min^{-1} and holding at this temperature for 1 h in an air atmosphere. The stabilized fibers were then carbonized by heating to 1,000 °C at a rate of 5 °C min^{-1} for 1 h in nitrogen.

2.2 Electrode preparation

The ground e-CNF was oxidized in a solution composed of 8 M HNO_3 and 2 M H_2SO_4 for 2 h under reflux to generate surface functional groups. The catalyst was then prepared by heating a solution H_2PtCl_6 (48.6 mg) in ethylene glycol (6.5 mL), following a previous procedure [15–18]. The pretreated e-CNF (200 mg) was then mixed with ethylene glycol (50 mL) under ultrasonication for 30 min. The Pt precursor solution was then slowly added dropwise into the beaker containing the sonicated, pretreated e-CNF. After the addition, a 1.0 M NaOH:ethylene glycol solution was slowly added until the pH was 12. The above solution was then heated in an oil bath at 130 °C for 3 h to replace the Pt. The Pt/e-CNF, of which 20 wt% was loaded Pt, was obtained by filtrating, washing, and drying with deionized water.

The first catalyst slurry was prepared by mixing 20 wt% Pt/e-CNF (or 20 wt% Pt/XC-72R, E-TEK), 5 wt% Nafion solution, and isopropyl alcohol. The slurry was coated on wet-proofed carbon paper (E-TEK) by a spray method. The slurry on carbon paper was then dried in oven at 80 °C for 30 min. The Pt loading was maintained at 0.5 mg cm^{-2} on both the anode and the cathode. The second slurry of Nafion was prepared by mixing 5 wt% Nafion solution with isopropyl alcohol at a 9:1 weight ratio of Pt:Nafion, and was then sprayed on the first catalyst slurry in order to enhance the adhesive strength between the membrane and electrodes. A membrane electrode assembly (MEA) of 5 cm^2 area was prepared by using Nafion 115 as a membrane under hot-pressing conditions of 140 °C and 1,500 psi for 100 s.

2.3 Characterization

Testing of the fuel cell was carried out using hydrogen and oxygen as reactants at 80 °C and 1 atm. The humidification temperatures of hydrogen and oxygen were maintained at 85 and 80 °C, respectively, under which the supplied gases were fully humidified. The feed rates of the reactant gases were 150 and 200 sccm for the hydrogen and oxygen electrodes, respectively.

The three-electrode test was carried out using a potentiostat/galvanostat (Won-A Tech., WBCS3000, Seoul, Korea). The working electrode was a thin layer of Nafion-impregnated catalyst cast on a carbon paper. The surface area of the carbon paper was 2.5 cm^2 and the catalyst loading was 0.5 mg cm^{-2}, based on this geometric area. Pt

wire and Ag/AgCl were used as a counter and reference electrode, respectively. The measurements were performed with a potential range −0.2 to 1.2 V and a scan rate of 10 mV s^{-1} in 1.0 M H_2SO_4 solution. The integrated coulombic charge for the reduction of the atomic hydrogen was evaluated by assuming a charge of Q_m (210 μC cm^{-2}) for the adsorption of hydrogen on smooth platinum. The adsorption/desorption charge (Q_H) of hydrogen was determined by subtracting the area of the double layer (Q_{DL}) from the total charge (Q_{Total}) between −0.2 and 0.1 V. The electrochemical surface area (ESA), chemical surface area (CSA), and efficiency of Pt utilization for the catalysts were calculated using following equations [19–24]:

$$Q_H = \frac{1}{2} \times (Q_{Total} - Q_{DL}) \quad (1)$$

$$ESA = \frac{Q_H\ [\mu C\ cm^{-2}]}{Q_m\ [\mu C\ cm^{-2}\ Pt] \times Pt\ loading\ [g\ cm^{-2}]} \quad (2)$$

$$CSA = \frac{6 \times 10^3}{d \times \rho} \quad (3)$$

$$Pt\ utilization\ (\%) = \frac{ESA}{CSA} \times 100 \quad (4)$$

where ρ (21.4 g cm^{-3}) is the density of Pt and d (nm) is the average diameter of the Pt particles.

The morphology of the nano-structured materials was examined by scanning electron microscopy (SEM, Hitachi, S-4700, Japan). The specific surface areas and pore size distributions of the samples were evaluated using the Brunauer, Emmett and Teller (BET) method and the Barrett, Joyner, Halenda (BJH) method (ASAP 2020 Micromeritics, Norcross, GA, USA). The X-ray diffraction (XRD) patterns were obtained using a D/MAX Uitima III (Rigaku, Tokyo, Japan). Transmission electron microscopy (TEM) images were obtained using a JEM-2000 FXII (JEOL, Peabody, MA, USA). The electrical conductivity of the sample in the plane direction was determined by a standard four-probe method. The electrical conductivity, σ, was calculated by using the following equation: $\sigma = L/(wtR)$, where R is the electrical resistance in Ω, w the sample width in cm, t the sample thickness in cm, and L the distance between the electrodes in cm.

3 Results and discussion

3.1 Morphology of e-CNF

Figure 1 shows SEM images of (a) the surface and (b) cross-section of e-CNF, carbonized at 1,000 °C for 1 h. The e-CNF had an average diameter of 250 nm that was aligned along the winding direction of the drum winder and appeared to be rough along the surface of carbon. In general, the fibrous nature of aligned e-CNF provides a high surface area as well as good connections between catalytic particles in the reaction layer. The e-CNF has high porous morphology because of its three-dimensional interconnected structure. High porous morphology provides a good performance of PEMFC caused by the increase in the gas diffusion rate. During the process of carbonization, organic materials undergo thermal pyrolytic decomposition and develop polyaromatic ring structures. The solid char is acquired in short-range order with the formation of distorted graphitic lamellae increasing with heat treatment. The localized and anisotropic densification leads to the development of very shallow pores with rough surfaces and electrical conductivity and improves overall Pt utilization.

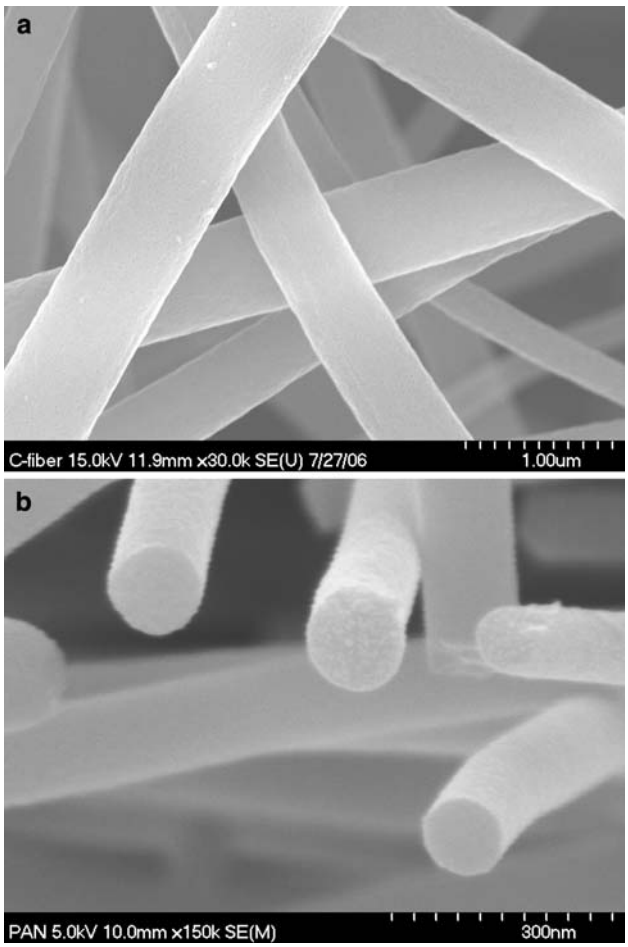

Fig. 1 SEM images of **a** the surface and **b** cross section of e-CNF carbonized at 1,000 °C

3.2 Pore size distribution

The important clue concerning Pt utilization can be obtained by analyzing the morphological information of Pt-free carbons (XC-72R, e-CNF) and Pt-supported carbons (Pt/XC-72R,

Table 1 Surface characterization of XC-72R and e-CNF

Sample	SSA ($m^2\ g^{-1}$)	V_{micro} ($cm^3\ g^{-1}$)	V_{meso} ($cm^3\ g^{-1}$)	V_{tot} ($cm^3\ g^{-1}$)	S_{micro} ($m^2\ g^{-1}$)	S_{meso} ($m^2\ g^{-1}$)	APD (nm)	Conductivity ($S\ cm^{-1}$)
XC-72R	235	0.062	0.578	0.640	156	79	10.92	4.5
e-CNF	307	0.128	0.054	0.182	292	15	2.36	9.9
Pt/XC-72R	194	0.049	0.550	0.599	132	62	14.28	–
Pt/e-CNF	302	0.125	0.053	0.178	288	14	2.31	–

SSA specific surface area, V_{micro} micropore volume, V_{meso} mesopore volume, V_{tot} total pore volume, S_{micro} micropore surface area, S_{meso} mesopore surface area, *APD* average pore diameter

Pt/e-CNF), as shown in Table 1. The morphology of XC-72R largely changed as Pt is loaded, whereas that of the e-CNF remained almost unchanged. The surface area of XC-72 was 235 $m^2\ g^{-1}$, while that of Pt/XC-72R begins to lower to 194 $m^2\ g^{-1}$ from the Pt particles easily penetrating into the mesopores of the XC-72R. Interestingly, the surface area of e-CNF was 307 $m^2\ g^{-1}$, whereas that of Pt/e-CNF was 302 $m^2\ g^{-1}$, the same as Pt-free e-CNF, because it is difficult for the Pt particles to penetrate the well-developed shallow pores. In detail, the mesopore volume and average pore diameter of the XC-72R and Pt/XC-72R were larger than those of e-CNF and Pt/e-CNF. Nevertheless, e-CNF and Pt/e-CNF had high surface areas, shallow pores with rough surfaces, and small average pore diameters, simultaneously, all suitable for enhancing Pt utilization. Figure 2 shows the mesopore size distribution (BJH method) of Pt-free carbons (XC-72R, e-CNF) and Pt-supported carbons (Pt/XC-72R, Pt/e-CNF) in the range 2–200 nm. XC-72R is granular particles known as commercial carbon, and e-CNF was carbonized at 1,000 °C for 1 h. XC-72R and Pt/XC-72R were mainly distributed in a range 2–200 nm, whereas e-CNF and Pt/e-CNF were mainly distributed as pore sizes from 2 to 4 nm, with a rough surface as a result of the electrospinning and carbonization. As mentioned above, the mesopore size distribution for XC-72R was considerably altered compared to that of Pt/XC-72R, on account of the development of mesopores. This results in lower Pt utilization. However, the profile of the mesopore size distribution between e-CNF and Pt/e-CNF does not show this change as the e-CNF was nearly void of developed mesopores, leading to improvement in Pt utilization. The XC-72R was mainly distributed in the all region between 2 to 200 nm, whereas e-CNF was mainly distributed as a shallow pore between 2 to 3 nm with a rough surface due to the electrospinning and carbonization. Figure 3 presents a schematic diagram of the fabrication process of the membrane electrode assembly (MEA), showing Pt penetration/exposure on XC-72R and e-CNF (including an SEM image of e-CNF). The XC-72R had a morphology giving low Pt utilization as it was difficult for the ionomer to form a three-phase boundary with Pt particles entering the mesopores, whereas the e-CNF had a good Pt-supported morphology by offering a high surface area and shallow pores with enhanced roughness due to the electrospinning and carbonization.

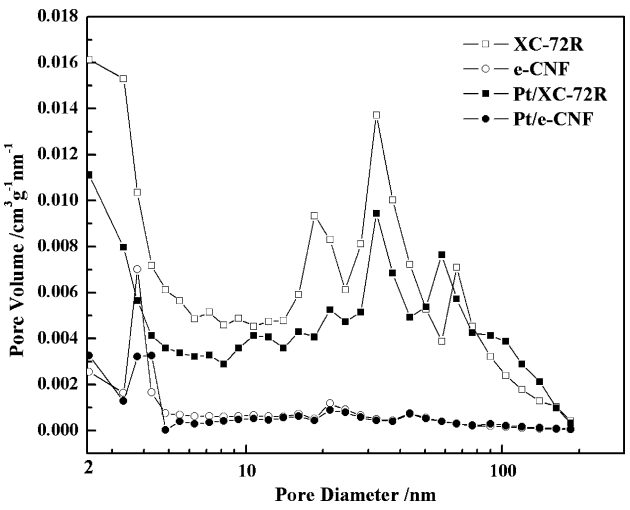

Fig. 2 Pore size distribution of XC-72R and e-CNF

3.3 Electrical conductivity

The electrical conductivity is highly significant in the performance of PEMFC. As shown in Table 1, the electrical conductivity of XC-72R was 4.5 $S\ cm^{-1}$, while that of e-CNF was 9.9 $S\ cm^{-1}$. The e-CNF prepared by electrospinning was a nanofiber aligned along a one-directional axis. The electronic conductivity is much higher along the axis of the fiber than across it because the resistance is minimized and the electrons are transferred easily along the aligned CNF. This leads to an improvement in PEMFC performance.

3.4 Analysis of XRD and TEM

Figure 4 shows the X-ray diffraction (XRD) patterns of Pt/XC-72R, Pt/e-CNF. All patterns gave the three characteristic peaks at $2\theta = 40$, 46, and 68° assigned to Pt(1 1 1), Pt(2 0 0), and Pt(2 2 0) planes, respectively. The crystalline Pt of two samples exhibited a face-centered cubic (fcc)

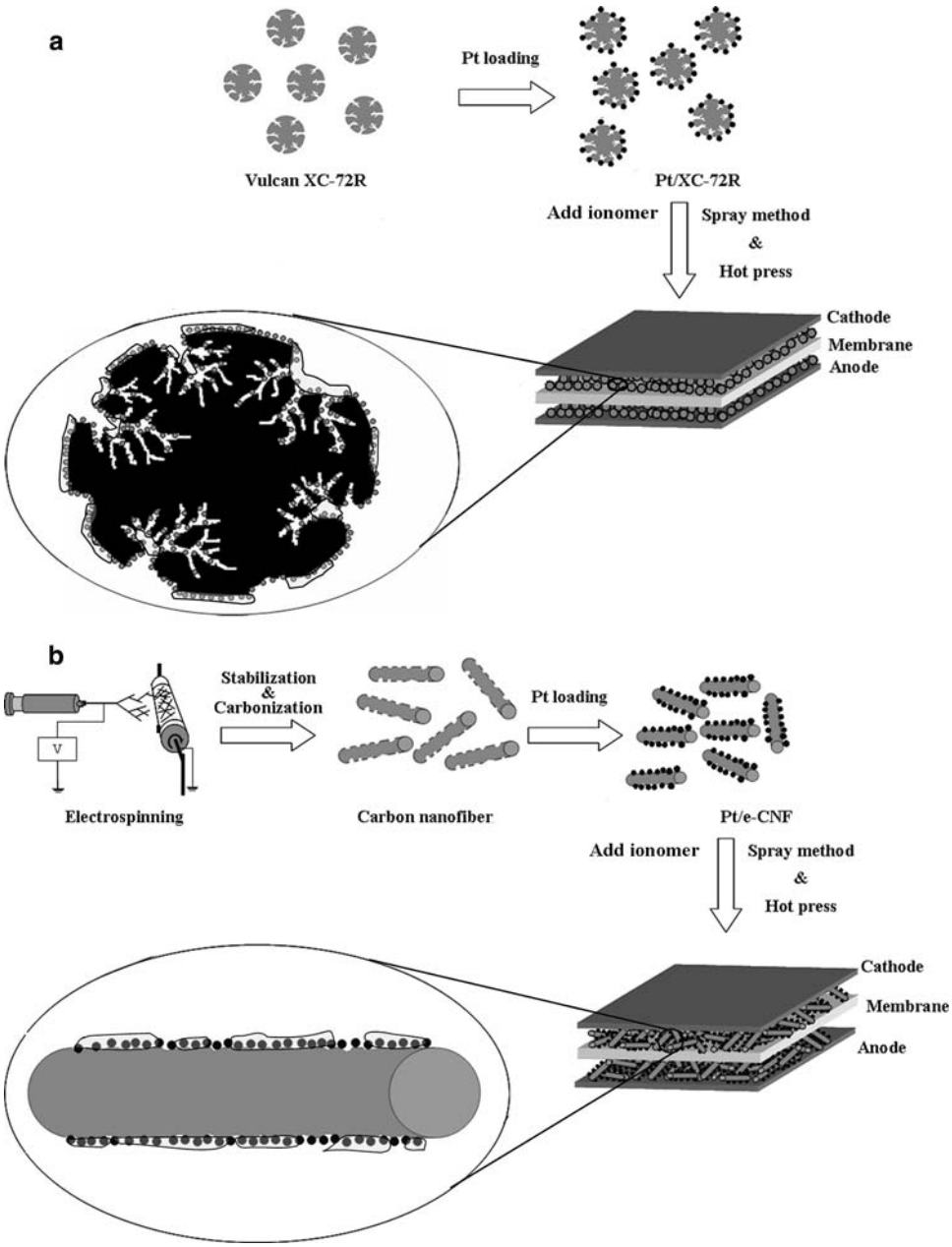

Fig. 3 Schematic diagrams of **a** Pt/XC-72R and **b** Pt/e-CNF

structure and the metal particle size was calculated by using the full width at half-maximum (FWHM) of the peak (2 2 0) from the Scherrer equation [25]. The particle sizes of Pt for Pt/XC-72R and Pt/e-CNF were 3.2 and 2.6 nm, respectively. Figure 5 shows the TEM images of the Pt/XC-72R and Pt/e-CNF for the morphology of the catalysts. All images show a uniform and high dispersion of Pt particles on the carbon surface (XC-72R or e-CNF). The Pt particles size on the carbon surface was measured with 200 particles chosen randomly from the TEM images. The average particle sizes of the Pt/XC-72R and Pt/e-CNF were 3.6 and 2.9 nm, respectively. The results by the TEM images are nearly consistent with the XRD analysis.

3.5 Electrochemical performance

Figure 6 shows the cyclic voltammograms (CV) of the Pt/XC-72R and Pt/e-CNF, at a scan rate of 10 mV s^{-1} in 1.0 M H_2SO_4 solution. The cathodic and anodic peaks between −0.2 and 0.1 V, versus Ag/AgCl, correspond to the adsorption and desorption of hydrogen ion Pt catalysts. Using the adsorption/desorption charge, electrochemical surface area (ESA), chemical specific surface area (CSA) and Pt utilization were calculated using Eqs. (1)–(4), with the results summarized in Table 2. Higher ESA indicates that Pt utilization is greater in the electrode reaction and leads to enhanced PEMFC performance. The ESA of Pt/e-CNF was

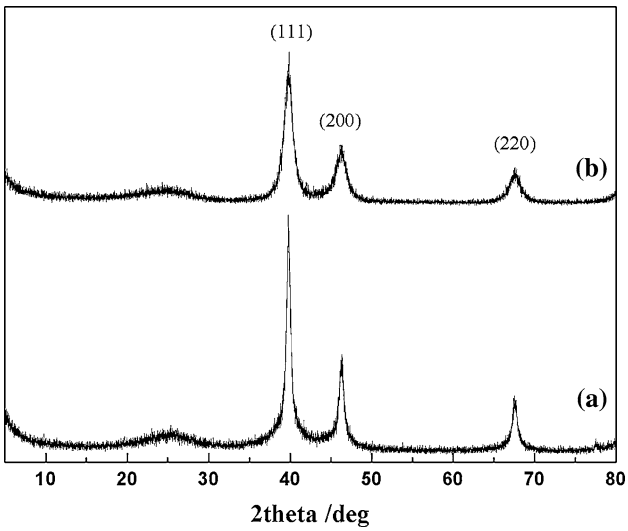

Fig. 4 XRD patterns of **a** Pt/XC-72R and **b** Pt/e-CNF

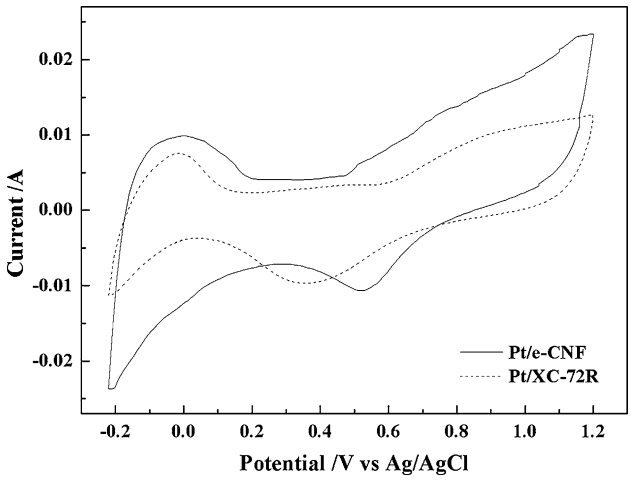

Fig. 6 Cyclic voltammograms of Pt/XC-72R and Pt/e-CNF at scan rate of 10 mV s^{-1} in 1 M H_2SO_4

approximately 2.4 times larger than that of Pt/XC-72R, as shown in Table 2. The Pt utilization was obtained by dividing ESA into CSA. Hence, the Pt utilization of the Pt/XC-72R and Pt/e-CNF electrodes was evaluated as 35% and 69%, respectively. The Pt utilization of Pt/e-CNF increased nearly two times compared with Pt/XC-72R.

3.6 Electrochemical impedance spectroscopy

Figure 7 shows the electrochemical impedance spectroscopy (EIS) curve by Nyquist plots in the range 20 mHz to 50 kHz for (a) Pt/XC-72R and (b) Pt/e-CNF electrodes. EIS provides the information concerning the charging/discharging process and electronic/ionic conductivity of electrode materials, and offers information on the equivalent series resistance (ESR). The intercept of the semicircle in the high frequency at the real axis represents the internal resistance (R_Ω), which is related to the electrical resistance of active materials [26]. The internal resistances of Pt/XC-72R and Pt/e-CNF electrodes were 0.27 and 0.49 Ω, respectively. This indicates that the use of e-CNF as catalyst support increases Pt utilization, because the e-CNF

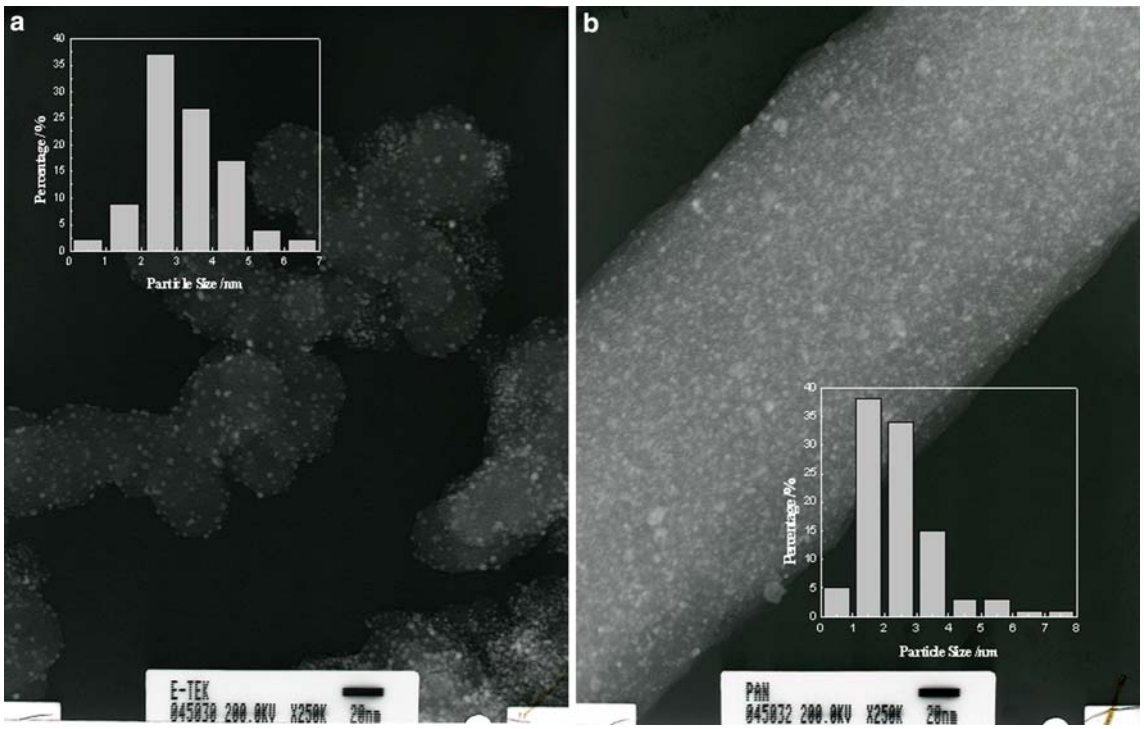

Fig. 5 TEM images of **a** Pt/XC-72R and **b** Pt/e-CNF

Table 2 The Pt particle size, RF, ESA, CSA and Pt utilization in XC-72R and e-CNF electrodes

	d_{TEM} (nm)	d_{XRD} (nm)	ESA (m^2 g^{-1} Pt)	CSA (m^2 g^{-1} Pt)	Pt utilization (%)
Pt/XC-72R	3.6	3.2	30.8	87.6	35.2
Pt/e-CNF	2.9	2.6	74.5	107.8	69.1

d_{TEM} Pt particle size by TEM, d_{XRD} Pt particle size by XRD, *ESA* electrochemical surface area, *CSA* chemical surface area

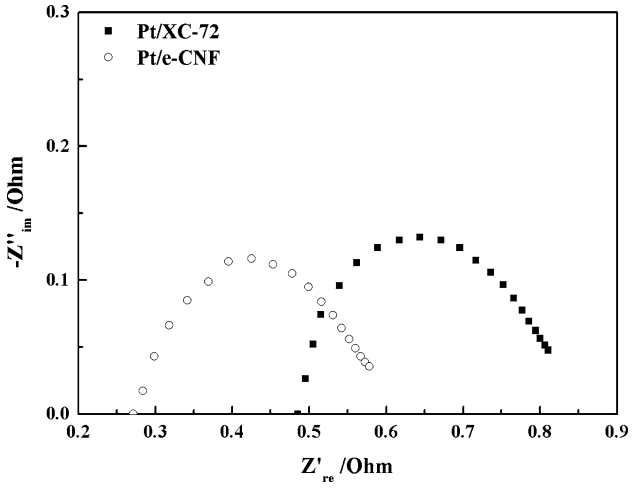

Fig. 7 Impedance plot of Pt/XC-72R and Pt/e-CNF

prepared by electrospinning and carbonation provides high surface area and shallow pores with rough surface.

3.7 Cell performance

Figure 8 shows the polarization and power density in the membrane electrode assembly (MEA) based on the Pt/XC-72R and Pt/e-CNF electrodes, as a function of current density. The Pt/e-CNF exhibits much higher performance than Pt/XC-72R over the whole current density range. The performance of Pt/e-CNF in the region of activation polarization (low current density) is higher than that of Pt/XC-72R. At 150 mA cm^{-2}, the cell voltage of Pt/e-CNF

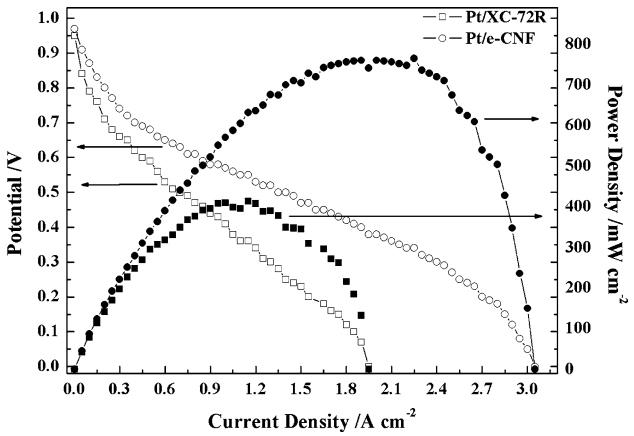

Fig. 8 Polarization curves and power density of MEAs with XC-72R and e-CNF

showed approximately 0.76 V, while that of Pt/XC-72R was near 0.83 V. This is why the effective activity of Pt is increased, indicating that the current density increased as small and abundant Pt particles are formed due to the e-CNF morphology. The performance of Pt/e-CNF in the region of ohmic polarization (low current density) is much better than that of Pt/XC-72R. At the same voltage (0.6 V), the current density of Pt/e-CNF increased approximately two times (900 mA cm^{-2}), compared to that of Pt/XC-72R (450 mA cm^{-2}). The reason for this is that the electronic conductivity of e-CNF is higher than that of XC-72R, in particular, the electronic conductivity is increased because e-CNF is aligned and has anisotropic structure. Furthermore, the performance of Pt/e-CNF in the region of mass transfer polarization (high current density) is much better than that of Pt/XC-72R. At the same voltage (0.2 V), the current density of Pt/XC-72R shows only 1,500 mA cm^{-2}, while that of Pt/e-CNF increased to 2,700 mA cm^{-2}. This is because the e-CNF protects the flooding of the electrode by forming a gas flow channel. Specifically, the aligned e-CNF provides better gas diffusion as the gas permeates easily between e-CNF layers. Conversely, the maximum power density of Pt/e-CNF increased nearly two times over to 0.765 W cm^{-2} at 2.25 A cm^{-2}, while that of Pt/XC-72R was 0.414 W cm^{-2} at 1.15 A cm^{-2}. The higher catalytic activity of Pt/e-CNF is due to its high surface area, shallow pores with rough surfaces, and enhanced electronic conductivity compared to Pt/XC-72R.

4 Conclusions

Electrospun PAN-based carbon nanofibers (e-CNF) were prepared through stabilization and carbonization as a Pt catalyst support. The partially aligned e-CNF, prepared by electrospinning and carbonization, had an excellent morphology and properties suitable for improving PEMFC performance. The e-CNF had high surface area and shallow pores with rough surfaces, whereas XC-72R had deep mesopores with small surface areas, indicating that PEMFC performance of the e-CNF was superior to that of XC-72R, through a three-phase boundary enhancement as high surface area and shallow pores with rough surfaces increase Pt utilization. The Pt particle size assessed by XRD in Pt/XC-72R was 3.2 nm, while that of Pt/e-CNF

was 2.6 nm. The Pt utilization of the Pt/e-CNF electrode was 69%, while that of Pt/XC-72R was 35%, giving higher catalytic activity for Pt/e-CNF and originating from high surface area, shallow pores with rough surfaces and enhanced electronic conductivity.

Acknowledgments This work was supported by the Korea Foundation for International Cooperation of Science & Technology (KICOS) through a grant provided by the Korean Ministry of Science & Technology (MOST) in K20602000009-07E0200-00910.

References

1. Fritts SD, Gopal R (1992) J Electrochem Soc 140:3347
2. Parthasarathy A, Srinivasan S, Appleby J, Martin CR (1992) J Electroanal Chem 339:101
3. Lemons RA (1990) J Power Sources 29:251
4. Uchida M, Aoyama Y, Tanabe M, Yanagihara N, Eda N, Ohta A (1995) J Electrochem Soc 142:2572
5. Roy SC, Christensen PA, Hamnett A, Thomas KM, Trapp V (1996) J Electrochem Soc 143:3073
6. Uchida M, Fukuoka Y, Sugawara Y, Eda N, Ohta A (1996) J Electrochem Soc 143:2245
7. Ye S, Vijh AK, Dao LH (1997) J Electrochem Soc 144:90
8. Liu Z, Gan LM, Hong L, Chen W, Lee JY (2005) J Power Sources 139:73
9. Park CH, Scibioh MA, Kim HJ, Oh IH, Hong SA, Ha HY (2006) J Power Sources 162:1023
10. Kim C, Park SH, Lee WJ, Yang KS (2004) Electrochim Acta 50:877
11. Kim C, Choi YO, Lee WJ, Yang KS (2004) Electrochim Acta 50:883
12. Oh GY, Ju YW, Kim MY, Jung HR, Kim HJ, Lee WJ (2008) Sci Total Environ 393:341
13. Ju YW, Choi GR, Jung HR, Kim C, Yang KS, Lee WJ (2007) J Electrochem Soc 154:A192
14. Oh GY, Ju YW, Jung HR, Lee WJ (2008) J Anal Appl Pyrolysis 81:211
15. Xu D, Zhang H, Ye W (2007) Catal Commun 8:1767
16. Li W, Liang C, Qiu J, Zhou W, Han H, Wei Z, Sun G, Xin Q (2002) Carbon 40:791
17. Huang HX, Chen SX, Yuan C (2008) J Power Sources 175:166
18. Guha A, Lu W, Zawodzinski TA, Schiraldi DA (2007) Carbon 45:1506
19. O'Hayre R, Lee SJ, Cha SW, Prinz FB (2002) J Power Sources 109:483
20. Escribano S, Aldebert P (1995) Solid State Ionics 77:318
21. Tamizhmani G, Dodelet JP, Guay D (1996) J Electrochem Soc 143:18
22. Li W, Zhou W, Li H, Zhou Z, Zhou B, Sun G, Xin Q (2004) Electrochim Acta 49:1045
23. Song S, Wang Y, Shen PK (2007) J Power Sources 170:46
24. Zeng J, Lee JY, Chen J, Shen PK, Song S (2007) Fuel cells 7:285
25. Warren BE (1969) X-ray diffraction. Addison-Wesley, Reading
26. Sreekumar TV, Liu T, Min BG, Guo H, Kumar S, Hauge RH, Smalley RE (2004) Adv Mater 16:58